Acta Cryst. (1979). A35, 975–989

The Defect Structure of VO_x. II. Local Ionic Arrangements in the Disordered Phase

BY M. MORINAGA* AND J. B. COHEN

Department of Materials Science and Engineering, The Technological Institute, Northwestern University, Evanston, IL 60201, USA

(*Received* 23 *January* 1979; *accepted* 2 *July* 1979)

Abstract

In VO_x ($0{\cdot}8 < x < 1{\cdot}3$), there are large numbers of cation and anion vacancies and interstitial vanadium ions. To determine the local arrangements of these defects, X-ray diffuse scattering was measured in absolute units with single crystals of VO_x ($x = 0{\cdot}89$, $1{\cdot}17$ and $1{\cdot}28$). For $x > 1$, the interstitials are present near vacancy clusters, similar to the defect arrays found in the semiconductor Fe_xO. For $x < 1$, there are few interstitials, but an increased concentration of anion vacancies. The anion and cation vacancies are arranged (so as to minimize the electrostatic energy) in rows along $\langle 110 \rangle$ directions with alternating vacancy-rich and vacancy-deficient $\{111\}$ layers. Some portions of this vacancy arrangement resemble that found in metallic TiO_x. VO_x behaves like a semimetal for $x < 1$, but a semiconductor for $x > 1$, and the present results, when compared to the defect structures in TiO_x and Fe_xO, show that the nature of the bonding between cations and anions controlling the conduction mechanism is reflected in the defect structure.

Introduction

Vanadium monoxide is stable over a wide range of compositions at high temperatures, from $VO_{0.8}$ to $VO_{1.3}$ (Schönberg, 1954; Andersson, 1954; Westman & Nordmark, 1960; Stenström & Westman, 1968). Its structure is similar to that of NaCl with large concentrations of vacancies on both anion and cation sublattices, which vary with composition (Banus & Reed, 1970; Banus, Reed & Strauss, 1972); even at stoichiometry about 15% of both sublattices are vacant. Interstitial (tetrahedrally coordinated) cations have been detected, their concentration increasing with oxygen content (Höier & Andersson, 1974; Watanabe, Andersson, Gjönnes & Terasaki, 1974; Morinaga & Cohen, 1976). The presence of composition-dependent diffuse scattering indicates that the defects are not randomly arranged (Andersson & Taftö, 1970; Hayakawa, Morinaga & Cohen, 1973; Andersson, Gjönnes & Taftö, 1974). There is an ordered phase $\sim VO_{1.2-1.3}$. For the most recent study of its structure see Morinaga & Cohen (1979), hereafter referred to as Part I of this study.

Andersson, Gjönnes & Taftö (1974) interpreted the diffuse scattering (determined with electron diffraction) from disordered $VO_{1.23}$ as due to tetrahedra of vacancies, each surrounding an interstitial vanadium ion in analogy to the defects found in Fe_xO (Koch & Cohen, 1969). However, the arrangement of clusters was not consistent with that found in the ordered phase; the nearest-neighbor intercluster vector was $(a_c/2)[211]$ (where a_c is the lattice parameter of the cubic disordered phase), shorter than the vector for the ordered phase, $(a_c/2)[221]$. Quantitative analysis of diffuse electron scattering is quite difficult. There are dynamical effects which complicate the mathematical representation and inelastic background scattering. These are affected by foil thickness and orientation, and absolute intensities are difficult to obtain. The diffuse scattering from VO_x is complex, and there are important contributions due to thermal and static ionic displacements ($\sim$15–30% even for $\sin\theta/\lambda < 0{\cdot}25$ Å^{-1} as will be shown below) which were assumed to be small by Andersson, Gjönnes & Taftö (1974). Furthermore, the clusters were *assumed* to exist, and the data, analyzed in terms of intercluster local order, were relative (not absolute) intensities.

The purpose of the present experiments is to analyze absolute diffuse X-ray intensities to obtain direct information on defect interactions and ionic displacements in single crystals of $VO_{0.89}$, $VO_{1.17}$, and $VO_{1.28}$. The relationship of these effects to the physical properties will be considered. VO_x is a semiconductor or a semimetal depending on its composition (Banus & Reed, 1970; Banus, Reed & Strauss, 1972). [The connection between the diffuse scattering and the Fermi surface of VO_x has already been examined (Hayakawa, Morinaga & Cohen, 1973).]

* Now at Toyohashi University of Technology, Toyohashi, Aichi 440, Japan.

0567-7394/79/060975-15$01.00

Experimental methods

Materials

The growth of the crystals and their analyses are described in Morinaga & Cohen (1976). After being held in flowing purified argon at 1323 K for several hours (in the presence of V metal foil to suppress oxidation), the crystals were cooled at ~273 K/min. Faces ~0·8 mm across were obtained by sectioning and polished using standard metallographic techniques and concluding with electrolytic polishing in a perchloric–methanol bath at room temperature (2–3 A, 10 V).

Diffraction techniques

These crystals were held in a vacuum (1·3–2·6 Pa) attachment to a GE quarter-circle goniostat; the cover was a thin Be hemisphere.

The measurement of diffuse scattering was carried out on an automated General Electric XRD-5 diffractometer (Schwartz, Morrison & Cohen, 1963), equipped with adjustable receiving and scatter slits for the diffracted beam. The incident beam was Cu $K\alpha$ radiation monochromated by a singly-bent pyrolitic graphite crystal, which focused at the detector in the vertical direction. The beam was smaller than the crystals' faces.

Beam divergences were determined by measuring the 200 Bragg reflection of a cleaved LiF single crystal. These corresponded to resolutions in reciprocal space of $\Delta h_{\text{horizontal}} = 0{\cdot}05$ r.l.u. and $\Delta h_{\text{vertical}} = 0{\cdot}07$ r.l.u. The measurements in a volume of reciprocal space were made at intervals of $\Delta h = 0{\cdot}1$. The X-ray tube was operated at 45 kV, 16 mA and intensities were measured with a scintillation counter with a pulse-height analyzer set to accept 90% of the Cu $K\alpha$.

Any variation of beam intensity for the long measuring times involved (about 21 d for each run) was monitored by a second detector, which recorded the fluorescent intensity produced when the incident beam passed through a thin Co foil (which attenuated the beam by ~12%). Measurements of the diffracted beam were made for a fixed number of monitor counts. (Typical measuring time was about 360 s for which the monitor recorded about 2×10^6 counts.) The variation of the direct beam, 4–5% over the period needed for measurements with each crystal, was corrected by the beam monitor.

The incident beam fluoresces vanadium and in addition there may be fluorescence from impurities in the sample. These fluorescent X-rays could distort the features of the diffuse scattering and to eliminate this radiation balanced filters of Ni and Co were employed. For this balancing the incident X-ray beam was Zr-filtered Mo radiation for radiation on the short wavelength sides of the filters ($\lambda < \lambda_{K_{Ni}}$), from a Bragg reflection of $VO_{1{\cdot}30}$. For radiation on the higher wavelength side ($\lambda > \lambda_{K_{Co}}$), the V fluorescence from $Vo_{1{\cdot}30}$ caused by the molybdenum incident radiation was employed. (By changing the setting of the pulse-height analyzer this radiation could be discriminated from the Mo $K\alpha$.) The effective thickness of the Ni filter was changed by tilting it around an axis perpendicular to the incoming beam. The difference in balancing was 1·4% for V fluorescence ($VK\alpha \times VK\beta$) and 0·9% for the Mo $K\alpha$. To check for any fluorescence with wavelengths between $\lambda_{K_{Ni}}$ and $\lambda_{K_{Co}}$, the energy spectrum of the background scattering was measured, without any filters, with a solid-state detector; no such scattering was detected.

A Ni foil was placed in front of the detector to improve the precision in taking the difference in intensities with the filters.

The direct beam power P_0 ($\sim 4 \times 10^7$ Hz) was determined by measuring the diffracted intensity from an Al powder briquette (Batterman, Chipman & DeMarco, 1961; Morinaga, 1978).

Under the same conditions as the measurements, the scattering from the air path and electronic background were measured as a function of 2θ by placing a lead beam trap at the specimen position. This corresponded to about 0·07–0·09 Hz, most of which was the noise of the electronics. There was no change in this component between the two filters within statistical error, so this term cancelled in taking the difference. The effect of surface roughness was determined using a method due to de Wolff (1956). The fluorescence produced by Mo $K\alpha$ was normalized at large 2θ angles. (The correction was 10–20% at 30° 2θ, depending on the specimen.) All data were corrected for the measured dead time (Schwartz & Cohen, 1977).

The ionicity of V and O appears to lie between neutral and singly-ionized states in the disordered phase (Morinaga & Cohen, 1976). Therefore, neutral atomic scattering factors (from Doyle & Turner, 1968) were employed in calculations. The present measurements were carried out in the range $0{\cdot}15 < \sin\theta/\lambda < 0{\cdot}40$. The dispersion corrections for V and O were taken from *International Tables for X-ray Crystallography* (1962). The Compton modified scattering was taken from Cromer (1969) and subtracted after correcting for Lorentz polarization, surface roughness, and placing the data on an absolute scale.

Scattering theory

Hayakawa & Cohen (1975) have derived general equations for the diffuse scattering from materials with multiple sublattices, including up to quadratic terms in atomic displacements.

The total coherent diffuse scattering intensity, I_D, in Laue units is given by

$$\begin{aligned} I_D(h)/I_{LM}(h) = {} & I_{SRO}(h) \\ & + h_1 Q_x(h) + h_2 Q_y(h) \\ & + h_3 Q_z(h) + h_1^2 R_x(h) \\ & + h_2^2 R_y(h) + h_3^2 R_z(h) \\ & + h_1 h_2 S_{xy}(h) + h_2 h_3 S_{yz}(h) \\ & + h_3 h_1 S_{zx}(h), \end{aligned} \quad (1)$$

where $h = (h_1,h_2,h_3)$ and h_1, h_2 and h_3 are continuous variables in reciprocal space. The term I_{LM} is the Laue monotonic scattering due to a random array of defects without displacements.

In (1), the first term on the right-hand side is the short-range order intensity $[I_{SRO}(h)]$, the next three terms are the size-effect scattering due to average interatomic displacements (whose components are in a direction indicated by the subscript) and the remaining terms are the first-order thermal diffuse scattering (TDS) plus Huang scattering (Huang, 1947) (due to mean square static displacements).

$$I_{SRO}(h) = \sum_l \sum_m \sum_n \bar{\alpha}_{lmn} \cos 2\pi(h_1 l + h_2 m + h_3 n), \quad (2a)$$

$$Q_x(h) = -\sum_l \sum_m \sum_n \bar{\gamma}^x_{lmn} \sin 2\pi(h_1 l + h_2 m + h_3 n), \quad (2b)$$

$$R_x(h) = \sum_l \sum_m \sum_n \bar{\delta}^x_{lmn} \cos 2\pi(h_1 l + h_2 m + h_3 n), \quad (2c)$$

$$S_{xy}(h) = \sum_l \sum_m \sum_n \bar{\varepsilon}^{xy}_{lmn} \cos 2\pi(h_1 l + h_2 m + h_3 n), \quad (2d)$$

with similar definitions for $Q_y(h)$, $R_y(h)$, $S_{yz}(h)$, $Q_z(h)$, $R_z(h)$ and $S_{zx}(h)$. The $\langle lmn \rangle$ are interatomic vectors defined by

$$\mathbf{r}_{lmn} = l\mathbf{a}_1 + m\mathbf{a}_2 + n\mathbf{a}_3, \quad (3a)$$

where $\mathbf{a}_1$, $\mathbf{a}_2$, and $\mathbf{a}_3$ are the usual cubic axes in real space. The diffraction vector $\mathbf{k}$ is given in terms of the axes $\mathbf{b}_i$ in reciprocal space:

$$\mathbf{k} = 2\pi(\mathbf{S} - \mathbf{S}_0)/\lambda = 2\pi(h_1 \mathbf{b}_1 + h_2 \mathbf{b}_2 + h_3 \mathbf{b}_3), \quad (3b)$$

where $\mathbf{S}$ and $\mathbf{S}_0$ are unit vectors in the directions of the scattered and incident beams, respectively, and λ is the wavelength of the X-rays.

The coefficients in the series, (2), are weighted averages of vectors spanning different sublattices. For example, the short-range order parameters $\bar{\alpha}_{lmn}$ are made up of terms involving

$$\alpha^{ij}_{\mu\nu}(lmn) = 1 - P^{ij}_{\mu\nu}/x^j_\nu, \quad (4)$$

where x^j_ν denotes the sublattice fraction of the jth component on the νth sublattice, and $P^{ij}_{\mu\nu}$ is the conditional probability of finding j-type atoms on the νth sublattice, separated by vector $\mathbf{r}_{lmn}$ from an i atom on the μth sublattice. The various sublattices in VO_x are shown in Table 1. For $m3m$ symmetry, sites labelled tetrahedral 1 and 2 are equivalent. The f.c.c. sites (F) are assumed to be occupied by oxygen ions, with vanadium ions in octahedral (O) and tetrahedral (T) sites. The three types of interatomic vectors are given in Table 2, which also indicates the sublattices that are spanned for each type of vector. With these values, and the known concentrations of defects (Morinaga & Cohen, 1976), the equations for the coefficients in (2) can be readily derived and are summarized in Tables 3 and 4, for the three compositions.* Note that for $VO_{0.89}$ there are no terms due to tetrahedral sites because the concentration of tetrahedral cations is essentially null.

* The details of the displacement terms for $VO_{1.28}$ are not actually analyzed in this paper and the equations for this composition are therefore not reported here; they may be found in Morinaga (1978).

Table 1. *Sublattice fractions and sublattice vectors for* VO_x

Type of sublattice	Sublattice vector	Sublattice fractions		
		Oxygen	Vanadium	Vacancy
f.c.c.	0,0,0	$x^O_F = 1 - c$	$x^M_F = 0$	$x^{V_O}_F = c$
Octahedral	$\frac{1}{2},\frac{1}{2},\frac{1}{2}$	$x^O_O = 0$	$x^M_O = 1 - a$	$x^{V_M}_O = a$
Tetrahedral 1	$\frac{1}{4},\frac{1}{4},\frac{1}{4}$	$x^O_{T_1} = 0$	$x^M_{T_1} = b$	$x^{V_M}_{T_1} = 1 - b$
Tetrahedral 2	$\frac{3}{4},\frac{3}{4},\frac{3}{4}$	$x^O_{T_2} = 0$	$x^M_{T_2} = b$	$x^{V_M}_{T_2} = 1 - b$

Vanadium = M, Oxygen = O, Vanadium vacancy = V_M, Oxygen vacancy = V_O. Vacancy concentration: $V_M = a$, $V_O = c$. In VO_x, tetrahedral sites have concentration $M = 2b$: $1/x = [(1 - a) + 2b]/(1 - c)$.

Table 2. *The three types of interatomic vectors in* VO_x *and the corresponding sublattice pairs*

	Type of *lmn*	Possible sublattice pairs
(1)	l, m, n all $[2p]/4$* $l + m + n = [4q]/4$	f.c.c.–f.c.c., Oct–Oct, Tet 1–Tet 1, Tet 2–Tet 2
(2)	l, m, n all $[2p]/4$ $l + m + n = [4q + 2]/4$	f.c.c.–Oct, Oct–f.c.c., Tet 1–Tet 2, Tet 2–Tet 1
(3)	l, m, n all $[2p + 1]/4$	f.c.c.–Tet 1, f.c.c.–Tet 2, Oct–Tet 1, Oct–Tet 2 Tet 1–f.c.c., Tet 2–f.c.c., Tet 1–Oct, Tet 2–Oct

* p and q are integers.

The x,y,z refer to the x,y,z components of the interatomic displacements from average sites of species i on μ, j on ν. Thus

$$\bar{\gamma}^x_{lmn} \propto \langle x^{ij}_{\mu\nu} \rangle_{ij}, \quad (5a)$$

$$\bar{\delta}^x_{lmn} \propto \langle x^i_\mu x^j_\nu \rangle, \quad (5b)$$

$$\bar{\varepsilon}^{xy}_{lmn} \propto \langle x^i_\mu y^j_\nu \rangle. \quad (5c)$$

Here, $x^{ij}_{\mu\nu} = x^i_\mu - x^j_\nu$, where x^i_μ is the displacement along the x direction of the ith atom on the μth sublattice.

The Borie–Sparks method (Borie & Sparks, 1971) has been applied to separate these terms in the diffuse scattering from alloys and oxides (Gragg & Cohen, 1971; Hayakawa, Morinaga & Cohen, 1973). This separation is based on the different symmetries of the terms in (1) and (2), and intensities at various h positions are added and subtracted to separate the terms. However, there are two difficulties with this procedure in this study. This method assumes that the scattering factor ratios that appear in Tables 3 and 4 are independent of $\sin\theta/\lambda$. But the minimum volume in reciprocal space for such a symmetry separation (Hayakawa & Cohen, 1975) in this case extends from 002 to 444. Furthermore, some 7000 points would need to be sampled if intervals of 0·1 were chosen, requiring over two months per crystal. Instead, (1) and (2) were solved by a least-squares procedure (Williams, 1972). Each series (2) was truncated, so that there were 50–90 total terms for the 2240 points sampled in the regions shown in Fig. 1. The stability of the results is sensitive to the measuring regions and the number of parameters, and tests of these variables will be presented with the results. Although not attempted by Williams, the scattering factor ratios can be represented by polynomials in terms of $\sin\theta/\lambda$, to examine if this variation is important; this will also be discussed.

Although the $\bar{\alpha}_{lmn}$ are combinations of several $\alpha^{ij}_{\mu\nu}$, Table 3, we wish to know the Warren short-range order parameters $\alpha^{ij}_{\mu\nu}$ from these $\bar{\alpha}_{lmn}$. We now consider if this is possible.

Table 3. *Laue monotonic scattering and* $\bar{\alpha}_{lmn}$

A. $VO^{*\dagger}_{0.89}$

Laue monotonic scattering	$x^0_F x^{V_0}_F f^2_0 + x^M_O x^{VM}_O f^2_M$
$\bar{\alpha}_{lmn}$ Type 1	$\dfrac{x^0_F x^{V_0}_F \alpha^{OV_0}_{FF} f^2_0 + x^M_O x^{VM}_O \alpha^{MVM}_{OO} f^2_M}{x^0_F x^{V_0}_F f^2_0 + x^M_O x^{VM}_O f^2_M}$
$\bar{\alpha}_{lmn}$ Type 2	$\dfrac{2x^M_O x^{V_0}_F \alpha^{MV_0}_{OF} f_0 f_M}{x^0_F x^{V_0}_F f^2_0 + x^M_O x^{VM}_O f^2_M}$
$\bar{\alpha}_{lmn}$ Type 3	0

B. $VO_{1.17}$

Laue monotonic scattering	$x^0_F x^{V_0}_F f^2_0 + (x^M_O x^{VM}_O + 2x^M_T x^{VM}_T) f^2_M$
$\bar{\alpha}_{lmn}$ Type 1	$\dfrac{x^0_F x^{V_0}_F \alpha^{OV_0}_{FF} f^2_0 + (x^M_O x^{VM}_O \alpha^{MVM}_{OO} + 2x^M_T x^{VM}_T \alpha^{MVM}_{TT}) f^2_M}{x^0_F x^{V_0}_F f^2_0 + (x^M_O x^{VM}_O + 2x^M_T x^{VM}_T) f^2_M}$
$\bar{\alpha}_{lmn}$ Type 2	$\dfrac{2x^M_O x^{V_0}_F \alpha^{MV_0}_{OF} f_0 f_M + 2x^M_T x^{VM}_T \alpha^{MVM}_{TT} f^2_M}{x^0_F x^{V_0}_F f^2_0 + (x^M_O x^{VM}_O + 2x^M_T x^{VM}_T) f^2_M}$
$\bar{\alpha}_{lmn}$ Type 3	$\dfrac{4x^M_T x^{V_0}_F \alpha^{MV_0}_{TF} f_0 f_M + 2(x^M_O x^{VM}_T \alpha^{MVM}_{OT} + x^M_T x^{VM}_O \alpha^{MVM}_{TO}) f^2_M}{x^0_F x^{V_0}_F f^2_0 + (x^M_O x^{VM}_O + 2x^M_T x^{VM}_T) f^2_M}$

C. $VO^{\ddagger}_{1.28}$

Laue monotonic scattering	$(x^M_O x^{VM}_O + 2x^M_T x^{VM}_T) f^2_M$
$\bar{\alpha}_{lmn}$ Type 1	$\dfrac{x^M_O x^{VM}_O \alpha^{MVM}_{OO} + 2x^M_T x^{VM}_T \alpha^{MVM}_{TT}}{x^M_O x^{VM}_O + 2x^M_T x^{VM}_T}$
$\bar{\alpha}_{lmn}$ Type 2	$\dfrac{2x^M_T x^{VM}_T \alpha^{MVM}_{TT}}{x^M_O x^{VM}_O + 2x^M_T x^{VM}_T}$
$\bar{\alpha}_{lmn}$ Type 3	$\dfrac{2(x^M_O x^{VM}_T \alpha^{MVM}_{OT} + x^M_T x^{VM}_O \alpha^{MVM}_{TO})}{x^M_O x^{VM}_O + 2x^M_T x^{VM}_T}$

* Assuming that $x^M_T = 0$.

† The scattering factor f_i in this table includes the temperature factor, taken from Morinaga & Cohen (1976).

‡ Assuming that $x^{V_0}_F = 0$.

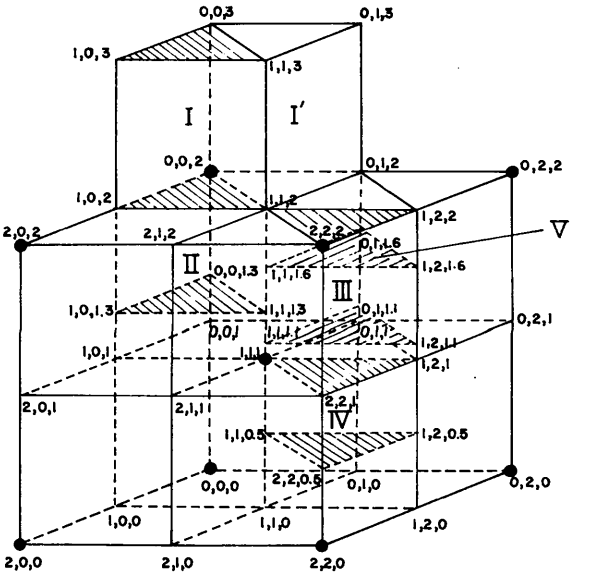

Fig. 1. Measured volumes in reciprocal space: $VO_{0.89}$ (I + II + III + IV), $VO_{1.17}$ (I + II + III + IV), $VO_{1.28}$ (I + II + III + V).

Table 4. $\bar{\gamma}^x_{lmn}$, $\bar{\delta}^x_{lmn}$ and $\bar{\varepsilon}^{xy}_{lmn}$

The scattering factor f_i in this table includes the temperature factor.

A. $VO_{0.89}$

$\bar{\gamma}^x_{lmn}$

Type 1*
$$\frac{2\pi}{N_1}[x_F^O f_O^2(x_F^O + x_F^{VO}\alpha_{FF}^{OVO})\langle x_{FF}^{OO}\rangle + x_O^M f_M^2(x_O^M + x_O^{VM}\alpha_{OO}^{MVM})\langle x_{OO}^{MM}\rangle]$$

Type 2: 0

Type 3: not involved

$\bar{\delta}^x_{lmn}$

Type 1
$$\frac{4\pi^2}{N_1}[x_F^O f_O^2(x_F^O + x_F^{VO}\alpha_{FF}^{OVO})\langle x_F^O x_F^O\rangle + x_O^M f_M^2(x_O^M + x_O^{VM}\alpha_{OO}^{MVM})\langle x_O^M x_O^M\rangle]$$

Type 2
$$\frac{4\pi^2}{N_1}[x_O^M x_F^O f_O f_M(1-\alpha_{OF}^{MO})\langle x_O^M x_F^O\rangle + x_F^O x_O^M f_O f_M(1-\alpha_{FO}^{OM})\langle x_F^O x_O^M\rangle]$$

Type 3: not involved

$\bar{\varepsilon}^{xy}_{lmn}$

Type 1
$$\frac{8\pi^2}{N_1}[x_F^O f_O^2(x_F^O + x_F^{VO}\alpha_{FF}^{OVO})\langle x_F^O y_F^O\rangle + x_O^M f_M^2(x_O^M + x_O^{VM}\alpha_{OO}^{MVM})\langle x_O^M y_O^M\rangle]$$

Type 2
$$\frac{8\pi^2}{N_1}[x_O^M x_F^O f_O f_M\{(1-\alpha_{FO}^{OM})\langle x_F^O y_O^M\rangle + (1-\alpha_{OF}^{MO})\langle x_O^M y_F^O\rangle\}]$$

Type 3: not involved

B. $VO_{1.17}$

$\bar{\gamma}^x_{lmn}$

Type 1†
$$\frac{2\pi}{N_2}[x_F^O f_O^2(x_F^O + x_F^{VO}\alpha_{FF}^{OVO})\langle x_{FF}^{OO}\rangle + f_M^2\{x_O^M(x_O^M + x_O^{VM}\alpha_{OO}^{MVM})\langle x_{OO}^{MM}\rangle + 2x_T^M(x_T^M + x_T^{VM}\alpha_{TT}^{MVM})\langle x_{TT}^{MM}\rangle\}]$$

Type 2
$$\frac{2\pi}{N_2}[2x_T^M(x_T^M + x_T^{VM}\alpha_{TT}^{MVM})\langle x_{TT}^{MM}\rangle f_M^2]$$

Type 3
$$\frac{2\pi}{N_2}[x_O^M(x_T^M + x_T^{VM}\alpha_{OT}^{MVM})\langle x_{OT}^{MM}\rangle f_M^2 + x_T^M(x_O^M + x_O^{VM}\alpha_{TO}^{MVM})\langle x_{TO}^{MM}\rangle f_M^2]$$

$\bar{\delta}^x_{lmn}$

Type 1
$$\frac{4\pi^2}{N_2}[x_F^O f_O^2(x_F^O + x_F^{VO}\alpha_{FF}^{OVO})\langle x_F^O x_F^O\rangle + f_M^2\{x_O^M(x_O^M + x_O^{VM}\alpha_{OO}^{MVM})\langle x_O^M x_O^M\rangle + 2x_T^M(x_T^M + x_T^{VM}\alpha_{TT}^{MVM})\langle x_T^M x_T^M\rangle\}]$$

Type 2
$$\frac{4\pi^2}{N_2}[x_F^O x_O^M f_O f_M(1-\alpha_{FO}^{OM})\langle x_F^O x_O^M\rangle + x_O^M x_F^O f_O f_M(1-\alpha_{OF}^{MO})\langle x_O^M x_F^O\rangle + 2x_T^M f_M^2(x_T^M + x_T^{VM}\alpha_{TT}^{MVM})\langle x_T^M x_T^M\rangle]$$

Type 3
$$\frac{8\pi^2}{N_2}[x_F^O x_T^M f_O f_M(1-\alpha_{FT}^{OM})\langle x_F^O x_T^M\rangle + x_T^M x_F^O f_O f_M(1-\alpha_{TF}^{MO})\langle x_T^M x_F^O\rangle + x_O^M f_M^2(x_T^M + x_T^{VM}\alpha_{OT}^{MVM})\langle x_O^M x_T^M\rangle + x_T^M f_M^2(x_O^M + x_O^{VM}\alpha_{TO}^{MVM})\langle x_T^M x_O^M\rangle]$$

$\bar{\varepsilon}^{xy}_{lmn}$

Type 1
$$\frac{8\pi^2}{N_2}[x_F^O f_O^2(x_F^O + x_F^{VO}\alpha_{FF}^{OVO})\langle x_F^O y_F^O\rangle + f_M^2\{x_O^M(x_O^M + x_O^{VM}\alpha_{OO}^{MVM})\langle x_O^M y_O^M\rangle + 2x_T^M(x_T^M + x_T^{VM}\alpha_{TT}^{MVM})\langle x_T^M y_T^M\rangle\}]$$

Type 2
$$\frac{8\pi^2}{N_2}[x_F^O x_O^M f_O f_M(1-\alpha_{FO}^{OM})\langle x_F^O y_O^M\rangle + x_O^M x_F^O f_O f_M(1-\alpha_{OF}^{MO})\langle x_O^M y_F^O\rangle + 2x_T^M f_M^2(x_T^M + x_T^{VM}\alpha_{TT}^{MVM})\langle x_T^M y_T^M\rangle]$$

Type 3
$$\frac{16\pi^2}{N_2}[x_F^O x_T^M f_O f_M(1-\alpha_{FT}^{OM})\langle x_F^O y_T^M\rangle + x_T^M x_F^O f_O f_M(1-\alpha_{TF}^{MO})\langle x_T^M y_F^O\rangle + x_O^M f_M^2(x_T^M + x_T^{VM}\alpha_{OT}^{MVM})\langle x_O^M y_T^M\rangle + x_T^M f_M^2(x_O^M + x_O^{VM}\alpha_{TO}^{MVM})\langle x_T^M y_O^M\rangle]$$

* $N_1 = x_F^O x_F^{VO} f_O^2 + x_O^M x_O^{VM} f_M^2$.

† $N_2 = x_F^O x_F^{VO} f_O^2 + (x_O^M x_O^{VM} + 2x_T^M x_T^{VM}) f_M^2$.

(i) $VO_{0.89}$ ($x_F^{V_O} = 22{\cdot}0$, $x_O^{V_M} = 12{\cdot}6$ *and* $X_T^M \simeq 0\%$)

(*a*) *Type* 1 *vectors*. The $\bar{\alpha}_{lmn}$ are combinations of $\alpha_{FF}^{OV_O}$ and $\alpha_{OO}^{MV_M}$. From the condition $0 \leq P_{\mu\nu}^{ij} \leq 1$, and from (4), and taking into account that the scattering was measured in the range $0{\cdot}15 < \sin\theta/\lambda < 0{\cdot}40$,

$$-6{\cdot}227 \leq x_O^M x_O^{V_M} \alpha_{OO}^{MV_M} f_M^2/(x_F^O x_F^{V_O} f_O^2 + x_O^M x_O^{V_M} f_M^2) \leq 0{\cdot}897 \quad (6)$$

and similarly for the term involving $\alpha_{FF}^{OV_O}$.

The $\bar{\alpha}_{lmn}$ can then be written:

$$\bar{\alpha}_{lmn} \simeq 0{\cdot}126\,\alpha_{FF}^{OV_O} + 0{\cdot}874\,\alpha_{OO}^{MV_M}, \quad (7)$$

for the present measurements (the values of f_O and f_M were those at $\sin\theta/\lambda = 0{\cdot}275$, the center of the measured regions although this choice does not affect the result appreciably). The two $\alpha_{\mu\nu}^{ij}$ cannot be separated, because the oxygen vacancies are major defects in $VO_{0.89}$.

(*b*) *Type* 2 *vectors*. From a similar analysis,

$$\bar{\alpha}_{lmn} \simeq 0{\cdot}933\,\alpha_{OF}^{MV_O}, \quad (8a)$$

or,

$$\alpha_{OF}^{MV_O} \simeq 1{\cdot}07\,\bar{\alpha}_{lmn}. \quad (8b)$$

Thus, $\alpha_{OF}^{MV_O}$ *can* be obtained directly from $\bar{\alpha}_{lmn}$.

There are no type 3 vectors (see Table 3).

(ii) $VO_{1.17}$ ($x_F^{V_O} = 4{\cdot}3$, $x_O^{V_M} = 23{\cdot}2$ *and* $x_T^M = 2{\cdot}5\%$)

(*a*) *Type* 1 *vectors*.

$$\bar{\alpha}_{lmn} \simeq 0{\cdot}016\,\alpha_{FF}^{OV_O} + 0{\cdot}773\,\alpha_{OO}^{MV_M} + 0{\cdot}211\,\alpha_{TT}^{MV_M}. \quad (9)$$

The $\bar{\alpha}_{lmn}$ is primarily due to $\alpha_{OO}^{MV_M}$, if $\alpha_{TT}^{MV_M}$ can be shown to be small. For such a case,

$$\alpha_{OO}^{MV_M} \simeq 1{\cdot}29\,\bar{\alpha}_{lmn}. \quad (10)$$

(*b*) *Type* 2 *vectors*.

$$\bar{\alpha}_{lmn} \simeq 0{\cdot}086\,\alpha_{OF}^{MV_O} + 0{\cdot}211\,\alpha_{TT}^{MV_M}. \quad (11)$$

From these equations, we cannot separate $\bar{\alpha}_{lmn}$ into $\alpha_{OF}^{MV_M}$ and $\alpha_{TT}^{MV_M}$.

(*c*) *Type* 3 *vectors*.

$$\bar{\alpha}_{lmn} \simeq 0{\cdot}006\,\alpha_{TF}^{MV_O} + 6{\cdot}489\,\alpha_{OT}^{MV_M} + 0{\cdot}050\,\alpha_{TO}^{MV_M}. \quad (12)$$

Thus, we can obtain $\alpha_{OT}^{MV_M}$:

$$\alpha_{OT}^{MV_M} \simeq 0{\cdot}15\,\bar{\alpha}_{lmn}. \quad (13)$$

(iii) $VO_{1.28}$ ($x_F^{V_O} = 0$, $x_O^{V_M} = 28{\cdot}0$ *and* $x_T^M = 3{\cdot}0\%$)

$$N_3 = x_O^M x_O^V + 2x_T^M x_T^{V_M} = 0{\cdot}260. \quad (14)$$

(*a*) *Type* 1 *vectors*.

$$\bar{\alpha}_{lmn} \simeq 0{\cdot}776\,\alpha_{OO}^{MV_M} + 0{\cdot}224\,\alpha_{TT}^{MV_M}. \quad (15)$$

If $\alpha_{TT}^{MV_M}$ is small,

$$\alpha_{OO}^{MV_M} \simeq 1{\cdot}29\,\bar{\alpha}_{lmn}. \quad (16)$$

(*b*) *Type* 2 *vectors*.

$$\bar{\alpha}_{lmn} \simeq 0{\cdot}224\,\alpha_{TT}^{MV_M}. \quad (17a)$$

Thus,

$$\alpha_{TT}^{MV_M} \simeq 4{\cdot}46\,\bar{\alpha}_{lmn}. \quad (17b)$$

(*c*) *Type* 3 *vectors*.

$$\bar{\alpha}_{lmn} \simeq 5{\cdot}376\,\alpha_{OT}^{MV_M} + 0{\cdot}065\,\alpha_{TO}^{MV_M}. \quad (18)$$

Thus,

$$\alpha_{OT}^{MV_M} \simeq 0{\cdot}19\,\bar{\alpha}_{lmn}. \quad (19)$$

Except for $VO_{1.28}$, some $\alpha_{\mu\nu}^{ij}$ can be obtained, but some cannot be explicitly determined. For $VO_{1.28}$, all the α's can be obtained. Similar reductions cannot be made for any of the displacement terms.

Results

Qualitative observations

Contour maps of the total coherent scattering (I_D/I_{LM}) in (1) (*i.e.* after all corrections) are shown in Figs. 2 and 3. For $VO_{0.89}$, there is a weak broad curved surface of diffuse scattering roughly perpendicular to a $\langle 110 \rangle$ direction with strong intensity near $\frac{111}{222}$ positions or their equivalent. (The position shifts off the $\langle 111 \rangle$

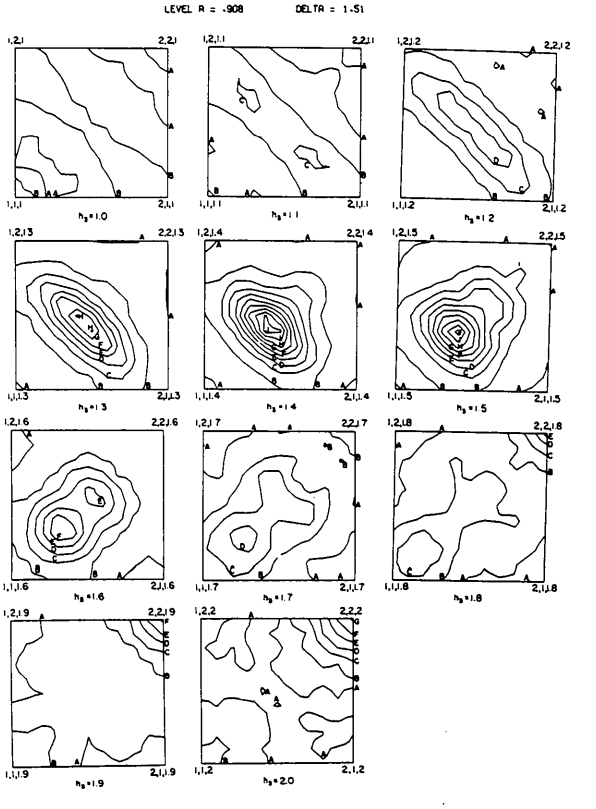

Fig. 2. Total coherent diffuse scattering (Laue units) for $VO_{0.89}$. The intensity contours increase with letters of the alphabet, with the increment delta = 1·51 (level A = 0·908).

line with increasing oxygen content.) These results suggest that the vanadium and/or the oxygen vacancies form linear arrays along ⟨110⟩ directions with vacancy rich and poor regions alternating in ⟨111⟩ directions (this will be discussed further below). The splitting of the diffuse intensity near $\frac{111}{222}$ for $x < 1$, observed in electron diffraction, is also apparent in the X-ray data.

Quantitative analysis

An example of the various least-squares analyses for each composition is summarized in Fig. 4 for $VO_{0.89}$. In addition to many combinations of terms, one run was made with one higher-order (h^3) displacement term, and one with the variation of the scattering factor included. In most runs, the weighting was unity, but in one, weighting proportional to the intensity was employed. In runs (*e*) and (*f*) average displacement terms (γ's) for type 2 vectors were included, even though these should be null as there are essentially no interstitials for this composition.

The trends are very much the same in all runs, and the same was true for the various displacement terms. In Fig. 5 the results for size coefficients (for type 1 and 2 vectors and for $VO_{0.89}$ and $VO_{1.17}$) are summarized by showing the extreme values in these solutions. For $VO_{1.17}$, α_{ooo} ranged from 0·0901 to 1·110. For $VO_{1.28}$ (not shown) this value (which should be unity by definition, equation 4) ranged from 0·7 to 1·01. For this crystal, as was noted in Fig. 1, different regions were measured, due to its orientation, region V instead of IV, both involving ~ 15% of the points. The $\bar{\alpha}_{lmn}$ for type 2 vectors were larger than their limiting values, since $\alpha_{TT}^{MV_M}$ must be less than unity. This indicates the occasional problems in the stability of the solution encountered with the least-squares procedure. Because of the similarity in the diffuse scattering in all crystals, the data in region V of $VO_{1.28}$ was replaced with that from region IV of $VO_{1.17}$ in one analysis, and added to it in another. These two results were similar and the results for $VO_{1.28}$ reported here were obtained with this procedure. (For further details, see Morinaga, 1978.) In what follows, we will therefore emphasize the results for $VO_{0.89}$ and $VO_{1.17}$ for which such problems did not arise.

In Part I of this study, the short-range order parameters for the ordered phase, $VO_{1.30}$, were obtained by integrating peaks in partial Patterson maps. These are shown in Fig. 6(*a*). For comparison, the short-range order parameters for $VO_{1.17}$ are shown in Fig. 6(*b*). The values are larger for the ordered phase but, particularly for type 1 and 3 vectors, there is good agreement in the variation *vs lmn*.

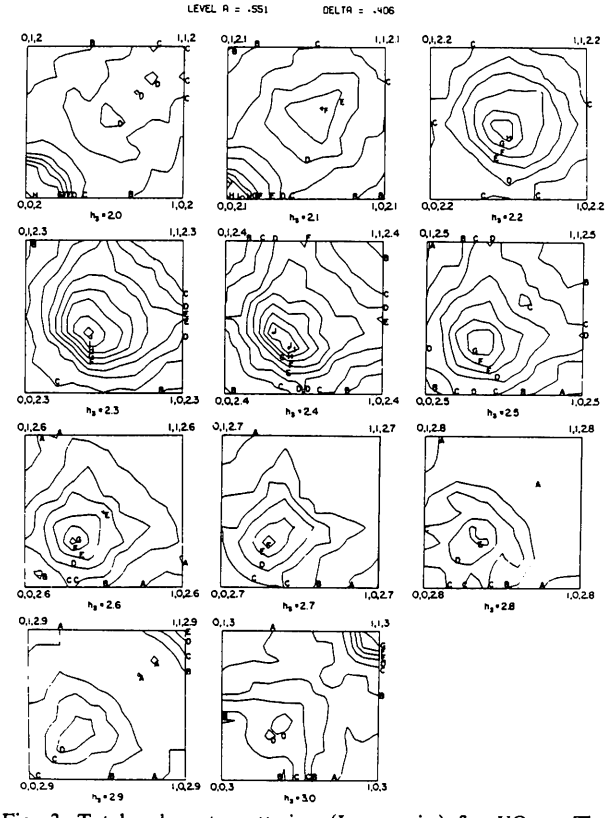

Fig. 3. Total coherent scattering (Laue units) for $VO_{1.17}$. The intensity contours increase with the letters of the alphabet, with the increment delta = 0·406 (level A = 0·551).

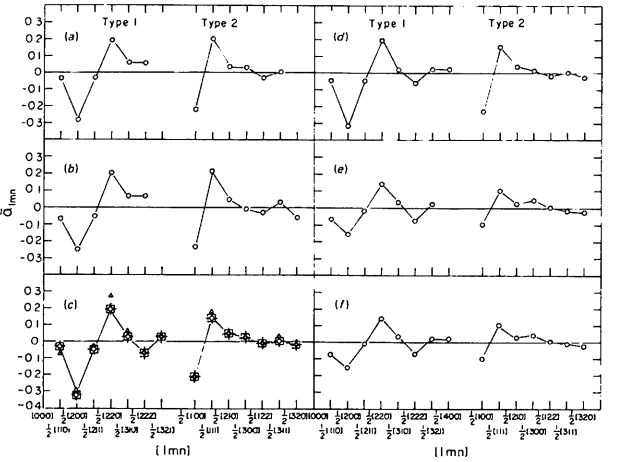

Fig. 4. Short-range order parameters $\bar{\alpha}_{lmn}$ *vs lmn* for $VO_{0.89}$. The number of terms of each type in the least-squares fit to the intensity is given in parentheses. (*a*) α_o, $\alpha_i(12)$, $\gamma_i(8)$, δ_o, $(\delta + \varepsilon)_i(36) = 58$; $\bar{\alpha}_{ooo} = 1{\cdot}656$, $R = 19{\cdot}5\%$. (*b*) α_o, $\alpha_i(13)$, $\gamma_i(8)$, δ_o, $(\delta + \varepsilon)_i(40) = 63$; $\bar{\alpha}_{ooo} = 1{\cdot}718$, $R = 18{\cdot}7\%$. (*c*) ○: α_o, $\alpha_i(14)$, $\gamma_i(11)$, δ_o, $(\delta + \varepsilon)_i(46) = 73$; $\bar{\alpha}_{ooo} = 1{\cdot}569$, $R = 15{\cdot}0\%$. +: α_o, $\alpha_i(14)$, $\gamma_i(11)$, δ_o, $(\delta + \varepsilon)_i(46) = 73$; h dependence of scattering factor terms, $\bar{\alpha}_{ooo} = 1{\cdot}570$, $R = 15{\cdot}0\%$. □: α_o, $\alpha_i(14)$, $\gamma_i(11)$, δ_o, $(\delta + \varepsilon)_i(46) = 74$; h^3 term included, $\bar{\alpha}_{ooo} = 1{\cdot}557$, $R = 15{\cdot}0\%$. △: α_o, $\alpha_i(14)$, $\gamma_i(11)$, δ_o, $(\delta + \varepsilon)_i(46) = 73$; weighting scheme, $\bar{\alpha}_{ooo} = 1{\cdot}504$, $R = 17{\cdot}5\%$. (*d*) α_o, $\alpha_i(15)$, $\gamma_i(12)$, δ_o, $(\delta + \varepsilon)_i(48) = 77$; $\bar{\alpha}_{ooo} = 1{\cdot}615$, $R = 14{\cdot}9\%$. (*e*) α_o, $\alpha_i(14)$, $\gamma_i(22)$, δ_o, $(\delta + \varepsilon)_i(46) = 84$; $\bar{\alpha}_{ooo} = 0{\cdot}873$, $R = 14{\cdot}2\%$. (*f*) α_o, $\alpha_i(15)$, $\gamma_i(23)$, δ_o, $(\delta + \varepsilon)_i(48) = 88$; $\bar{\alpha}_{ooo} = 0{\cdot}862$, $R = 14{+}2\%$. (*e*) and (*f*) include $\bar{\gamma}$ terms for type 2 vectors.

The diffuse intensity synthesized from the coefficients is compared to an electron diffraction pattern in Fig. 7. The main features are all well reproduced.

Synthesized components of the diffuse intensity are presented in Figs. 8 and 9, which may be compared to Figs. 2 and 3 respectively. There is good agreement in shape and relative magnitude.

We conclude then that, with proper care in the analysis, it is possible to obtain local order parameters for such a complex system. The R indices comparing the fit of the parameters in the least-squares solution to the measured intensity is ~14% for $VO_{0.89}$ (see Fig. 4) and 8% for $VO_{1.17}$, compared to expected values of ~6%. In Tables 5–7 the $\alpha^{lj}_{\mu\nu}$ are presented for those vectors for which these can be obtained from the $\bar{\alpha}$'s unambiguously. The $\bar{\alpha}$ were small for tetrahedral

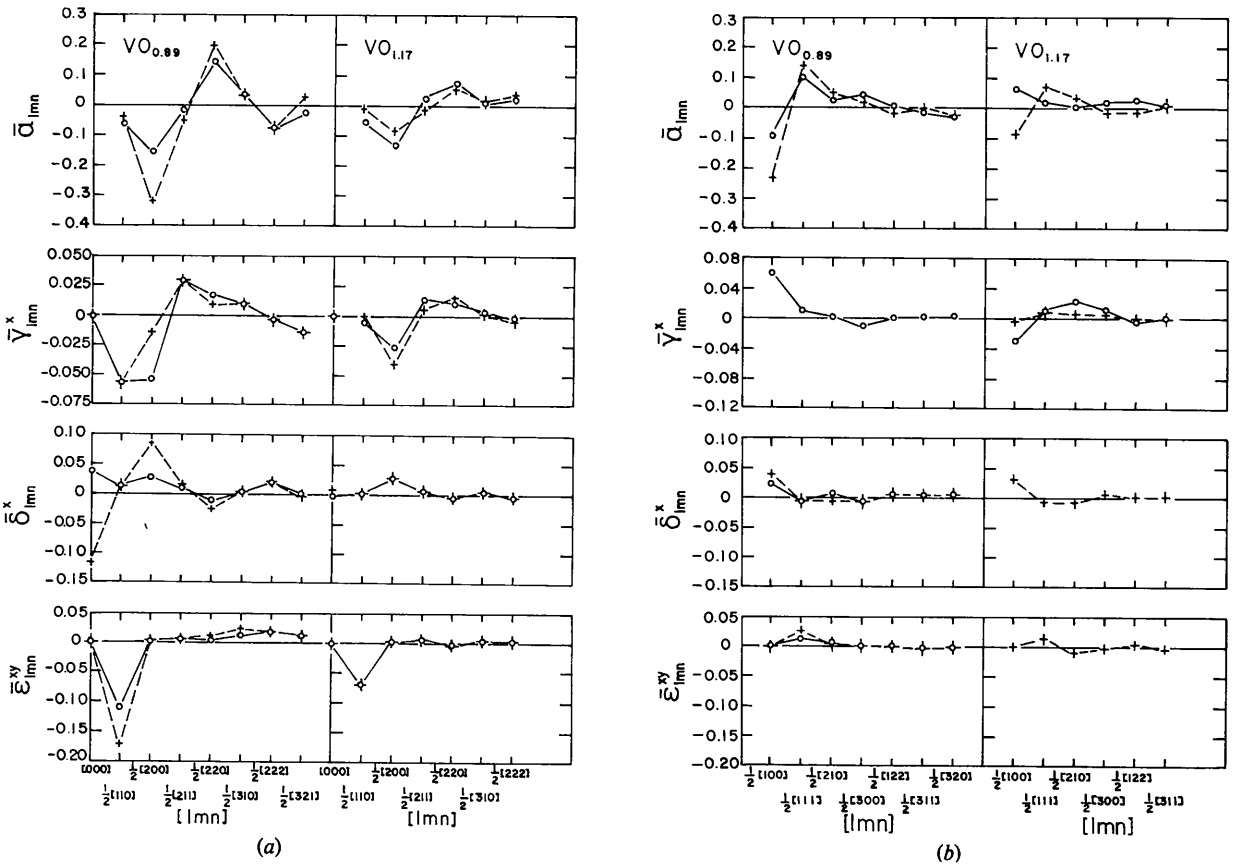

Fig. 5. Summary of $\bar{\alpha}_{lmn}$, $\bar{\gamma}_{lmn}$, $\bar{\delta}_{lmn}$ and $\bar{\varepsilon}_{lmn}$ for $VO_{0.89}$ and $VO_{1.17}$ for type 1 vectors (*a*) and for type 2 vectors (*b*). The dotted and solid lines correspond to extreme values in the least-squares solutions.

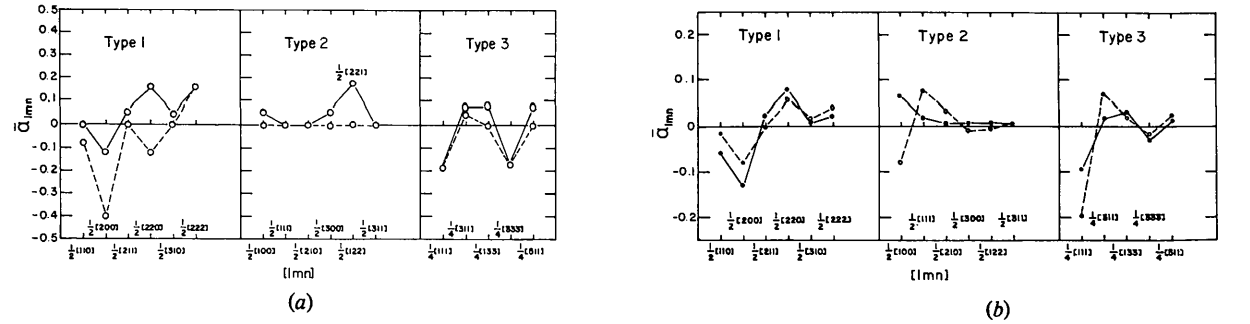

Fig. 6. (*a*) Short-range order parameters, $\bar{\alpha}_{lmn}$, *vs lmn* for ordered phase $VO_{1.30}$, from Part I. As the ordered phase is a tetragonal phase, there are several non-equivalent vectors for each *lmn*; the largest $\bar{\alpha}_{lmn}$ is indicated by a solid line, and the smallest one is shown by a dotted line. (*b*) Short-range order parameters $\bar{\alpha}_{lmn}$ *vs lmn* for $VO_{1.17}$. ● α_O, $\alpha_l(17)$, $\bar{\gamma}_l(25)$, δ_O, $(\delta + \varepsilon)_l(36)$, ○ α_O, $\alpha_l(17)$, $\gamma_l(25)$, δ_O, $(\delta + \varepsilon)_l(18)$.

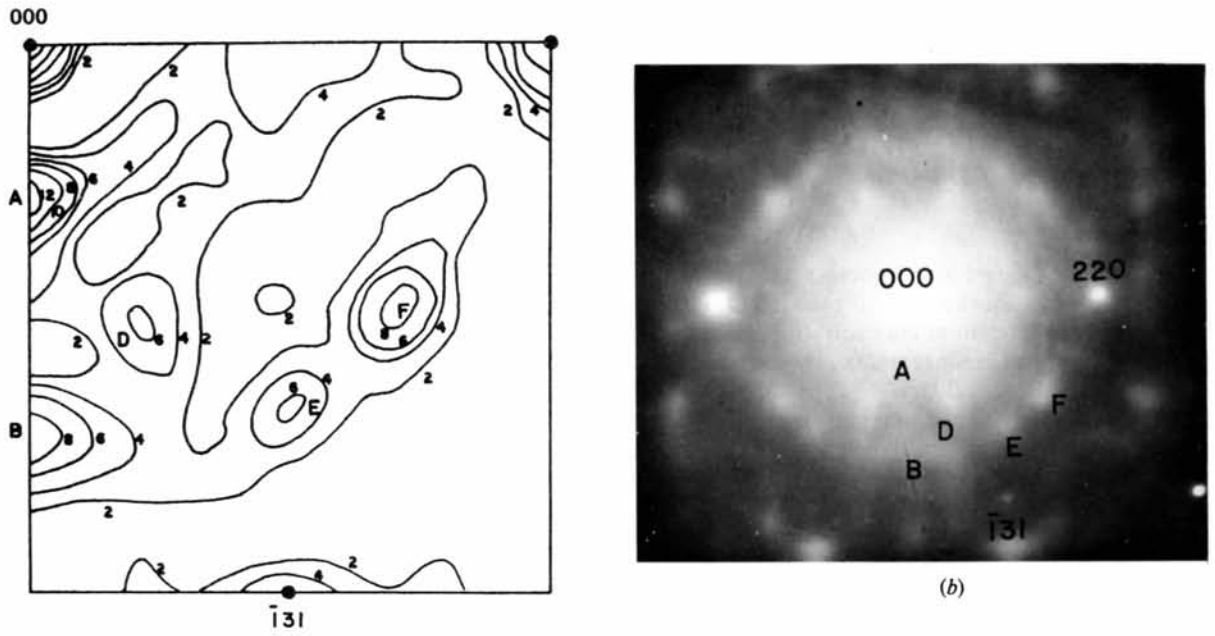

Fig. 7. (*a*) Synthesized total diffuse intensity on the (1$\bar{1}$4) plane of the reciprocal lattice for $VO_{0.89}$. (*b*) Electron diffraction pattern near the (1$\bar{1}$4) plane of $VO_{1.02}$. (Diffuse scattering is similar to that of $VO_{0.89}$.)

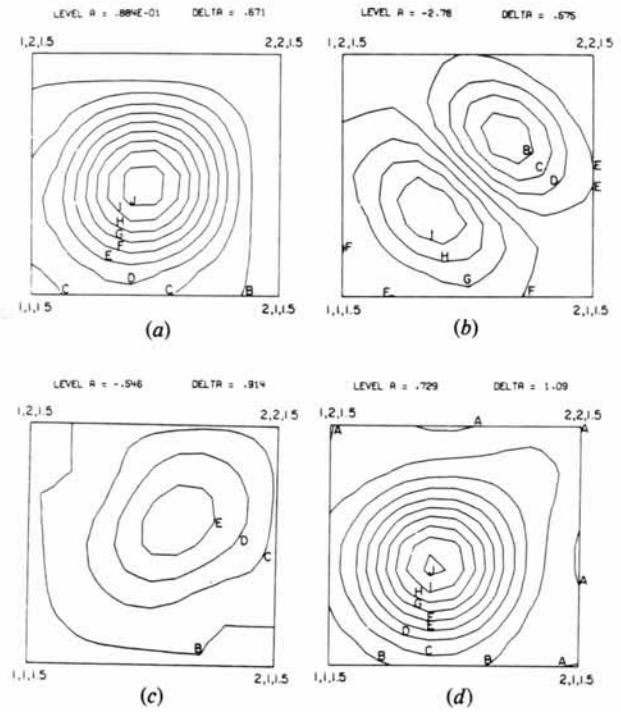

Fig. 8. Synthesized components of diffuse scattering for $VO_{0.89}$: (*a*) short-range order intensity; (*b*) first-order size-effect scattering; (*c*) thermal diffuse scattering + Huang scattering; (*d*) synthesized total diffuse scattering.

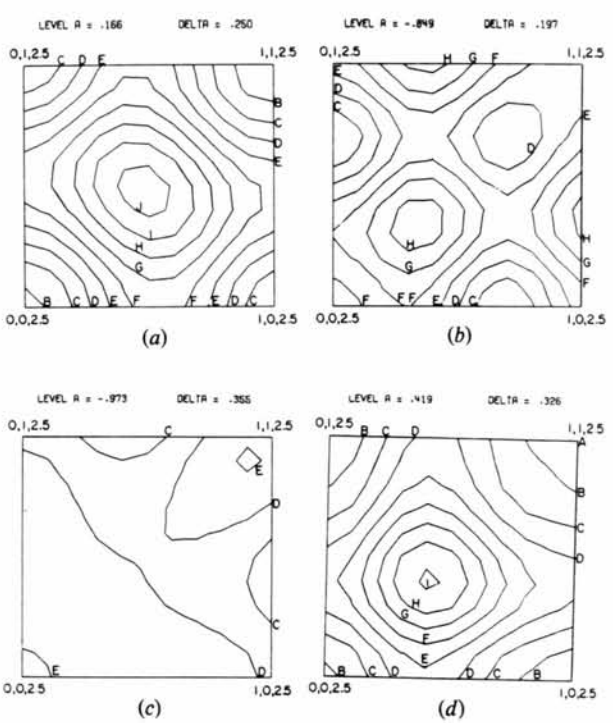

Fig. 9. Synthesized components of diffuse scattering for $VO_{1.17}$: (*a*) short-range order intensity; (*b*) first-order size-effect scattering; (*c*) thermal diffuse scattering + Huang scattering; (*d*) synthesized total diffuse scattering.

vectors in $VO_{1.17}$ (see Fig. 6*b*) so that $\alpha_{OO}^{MV_M}$ could be obtained for this composition. (Compare the type 2 interatomic vectors $\langle\frac{1}{2}00\rangle$, $\langle\frac{3}{2}00\rangle$ and $\langle\frac{11}{22}1\rangle$.)

Discussion

Local order

The $\bar{\alpha}_{lmn}$ for types 1 and 3 vectors are similar for all compositions and for the ordered phase, $VO_{1.30}$, despite the variation in interstitial concentration, and therefore the local atomic arrangements should be similar. However, for $a_c/2$ $\langle 221\rangle$, a type 2 vector, $\alpha_{TT}^{MV_M}$ between interstitial vanadium ions is positive for the ordered phase but small for the disordered phase. In the ordered state (see Part I) there are periodic tetrahedra of vacancies occluding an interstitial ion and these interstitials are separated by this vector; apparently these interstitials are more randomly distributed above the critical temperature, as mentioned above.

The $\bar{\alpha}_{lmn}$ for type 1 vectors involve sites on the cation, anion and tetrahedral interstitial sublattices, not between them. The near-zero values of $\bar{\alpha}$ for first- and third-neighbor vectors indicate that there is a near-random distribution of defects around a defect in these shells, but unlike species (say a vanadium ion and a vacancy) at the ends of the vector are favoured for second neighbors ($\bar{\alpha}$ negative) and like species for the fourth shell ($\bar{\alpha}$ positive). An ideal model for a domain, which fits these criteria for the oxygen-rich compositions (which contain primarily vanadium vacancies) and the qualitative features of the overall diffuse scattering, is shown in Fig. 10. Note that at the second-neighbor position from a vanadium ion (A_1) a vanadium vacancy occurs (C_1), whereas at the fourth-neighbor position there is another cation (at another A_1 site). At first- and third-neighbor positions the sites are

Table 5. $\alpha_{OF}^{MV_O}$ *for* $VO_{0.89}$

Type 2 $4\times[lmn]$	(*a*) $\bar{\alpha}_0 = 1.569$	(*b*) $\bar{\alpha}_0 = 0.873$	Average
200	−0.243	−0.101	−0.172
222	0.155	0.115	0.135
420	0.054	0.023	0.038
600	0.023	0.047	0.035
244	−0.018	0.003	−0.007
622	0.001	−0.013	−0.006
640	−0.022	−0.027	−0.025

Table 6. $\alpha_{\mu\nu}^{ij}$ *for* $VO_{0.17}$

Type 1 $4\times[lmn]$	(*a*) $\alpha_{OO}^{MV_M}$ $\bar{\alpha}_0 = 0.901$	(*b*) $\alpha_{OO}^{MV_M}$ $\bar{\alpha}_0 = 1.11$	Average
220	−0.023	−0.076	−0.049
400	−0.111	−0.172	−0.141
422	−0.002	0.027	0.013
440	0.072	0.102	0.087
620	0.021	0.009	0.015
444	0.050	0.027	0.038
Type 3 $4\times[lmn]$	(*a*) $\alpha_{OT}^{MV_M}$	(*b*) $\alpha_{OT}^{MV_M}$	Average
111	−0.030	−0.016	−0.023
311	0.010	0.000	0.005
133	0.002	0.004	0.003
333	−0.004	−0.006	−0.005
511	0.004	0.002	0.003

Table 7. $\alpha_{\mu\nu}^{ij}$ *for* $VO_{1.28}$ ($\bar{\alpha}_0 = 0.70$)

Type 1 $4\times[lmn]$	$\alpha_{OO}^{MV_M}$	Type 2 $4\times[lmn]$	$\alpha_{TT}^{MV_M}$	Type 3 $4\times[lmn]$	$\alpha_{OT}^{MV_M}$
220	−0.039	200	0.241	111	−0.022
400	−0.184	222	0.013	311	0.012
422	0.022	420	0.100	133	0.018
440	0.100	600	0.163	333	0.002
620	0.057	244	0.106	511	0.022
444	0.023	622	0.085		

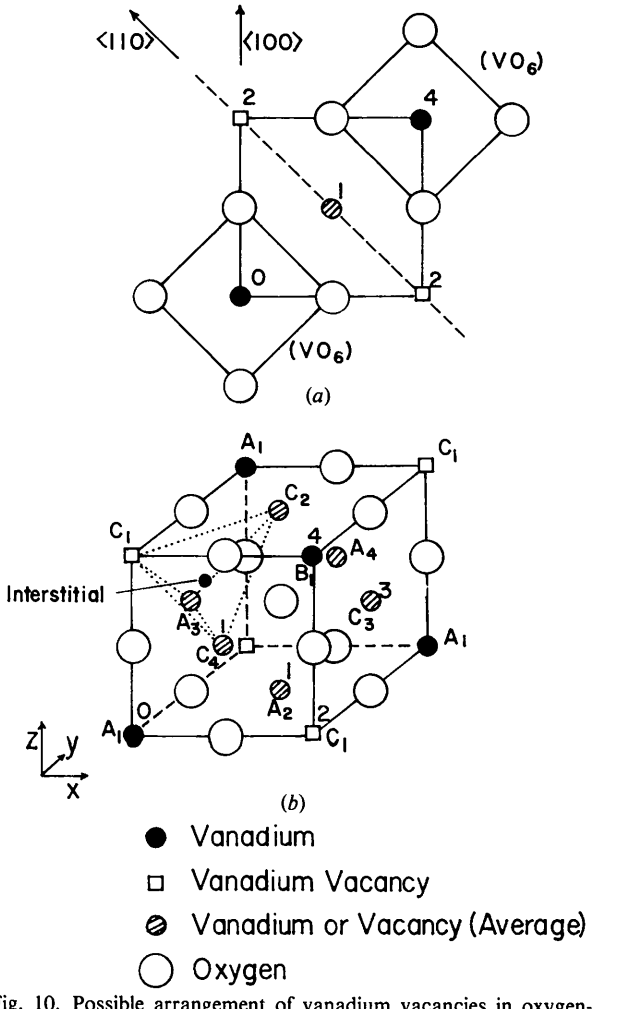

Fig. 10. Possible arrangement of vanadium vacancies in oxygen-rich VO_x (*a*) on the (100) plane (neighbor shells are numbered); (*b*) a three-dimensional model.

filled with vacancies or cations proportional to their average concentration (that is a random arrangement). Because $\alpha_{OT}^{MV_M}(\frac{111}{444})$ is negative (Tables 6 and 7), interstitial vanadium ions must be nearest neighbors to cation vacancies.

We can proceed further with this idealized model for the local atomic arrangements by considering the theory of stacking of ions on the closely packed {111} planes in oxides by Iida (1955). There are two physically significant ways to divide the lattice sites on {111} planes into several sublattices. One set is indicated by subscripts on the (lettered) layers in Fig. 11 for the model in Fig. 10, and a possible stacking sequence for these layers is presented in Table 8. The

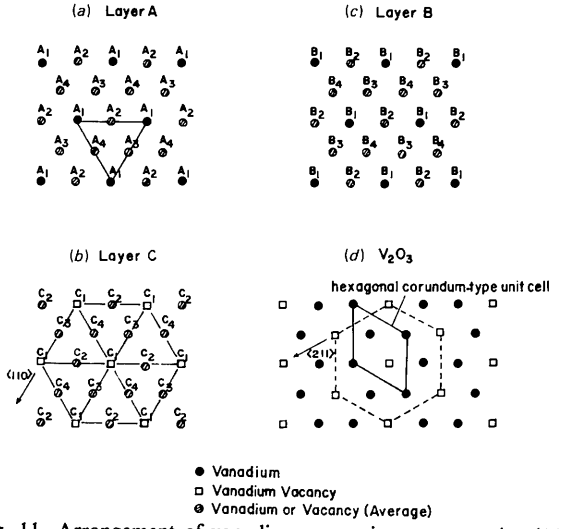

Fig. 11. Arrangement of vanadium vacancies on successive (111) planes in the model in Fig. 10: (*a*) layer *A*, (*b*) layer *C*, (*c*) layer *B*, (*d*) the V_2O_3 structure.

Table 8. *Possible stacking sequence of vanadium vacancies in* $VO_{1.17}$

Z*				
0	O†	*TC*		
$\frac{1}{2}$	*M*		$T\mathbf{A}_1$‡	$(TA_2 + TA_3 + TA_4)$
1	O	*TB*		
$1\frac{1}{2}$	*M*		$(TC_2 + TC_3 + TC_4)$	TC_1§
2	O	*TA*		
$2\frac{1}{2}$	*M*		$T\mathbf{B}_1$	
3	O	*TC*		
$3\frac{1}{2}$	*M*		$(TA_2 + TA_3 + TA_4)$	TA_1
4	O	*TB*		
$4\frac{1}{2}$	*M*		$T\mathbf{C}_1$	$(TC_2 + TC_3 + TC_4)$
5	O	*TA*		
$5\frac{1}{2}$	*M*		$(TB_2 + TB_3 + TB_4)$	TB_1
6	O	*TC*		

* Z is the height of the {111} closed-packed plane.

† *M* means vanadium ion and O means oxygen ion.

‡ $T\mathbf{A}_1$ at $\frac{1}{2}$ indicates that the vanadium ions preferentially occupy the A_1 sites, whereas $(TA_2 + TA_3 + TA_4)$ are sites of average vacancy occupation.

§ TC_1 at $1\frac{1}{2}$ indicates that the vanadium vacancies are preferentially in C_1 sites, whereas $(TC_2 + TC_3 + TC_4)$ are sites of average vacancy occupation.

preferential occupation of vanadium ions required by the α's at A_1 sites in Fig. 10(*b*) would yield a different electrostatic potential at C_1 sites from that at other sites, which would induce vacancies at *C* sites, to obtain local charge balance. (Compared to random occupation, a vanadium ion at A_1 sites has an effective positive charge while a vacancy at C_1 is negative.) Similarly, because of the presence of vacancies at C_1 sites, the B_1 sites are also occupied by vanadium ions. Thus this arrangement helps satisfy local charge neutrality and minimizes the increase of electrostatic energy due to the vacancies (Goodenough, 1972). (The role of the interstitials will be discussed in the next section.)

The perodicity is twice that of the basic NaCl cell, which would account for the strong diffuse intensity at $\frac{111}{222}$. A similar stacking arrangement for vanadium-rich compositions, for which there are both anion and cation vacancies, is given in Table 9. A three-dimensional model appears in Fig. 12. In this model, $\alpha_{OF}^{MV_O}(\frac{111}{222}) > 0$, in agreement with Table 5. Such a domain model is obviously ideal. Firstly, it involves 25% vanadium and oxygen vacancies on site 1, but the actual concentrations are less (13–22%). Also, the $\bar{\alpha}_{lmn}$ are larger for type 1 vectors in $VO_{0.89}$ than in $VO_{1.17}$, so that the tendency to the model must vary with composition. Only the signs of the $\bar{\alpha}$'s have been employed in forming the model, not the actual magnitudes. In order to test this construction further, a computer simulation was obtained for 4000 sublattice sites in three dimensions (Gehlen & Cohen, 1965; Gragg, 1970), employing the first six $\alpha_{FF}^{OV_O}$ for $VO_{0.89}$ (assuming $\bar{\alpha}_{lmn} = \alpha_{FF}^{OV_O}$), and the $\alpha_{OO}^{MV_M}$ for $VO_{1.17}$ and $VO_{1.28}$. The vacancies and ions in the simulations were exchanged until they fit the measured α values to 1%. Also, a near-random simulation (with interchanges until $\alpha_1 - \alpha_6 \simeq 0$) was examined for comparison. The results are as follows:

(*a*) Some 50% of the vacancies have no second-neighbor vacancies, in agreement with the model (compared to ~20% in the random model).

(*b*) The percent of vacancies having near-random arrangements of vacancies and ions in the first and third shells but 5–6 ions in the second shell, as in the model in Fig. 10(*b*), is 40% in the simulation with the measured α's compared to 20% in the random simulation.

(*c*) There are alternating vacancy-rich and vacancy-poor {111} planes in the simulations.

(*d*) The number of near-neighbor quadruplets of vacancies, or quadruplets with three out of four sites vacant, is approximately half that in the random state, a further indication of the tendency for the vacancies to be isolated.

(*e*) For the models for $VO_{1.17}$ and $VO_{1.28}$, the interstitial occupation is such that 200 and 240 such sites in the 4000-atom model would be occupied. In the simulations there are 201 and 410 near-neighbor

tetrahedra of cation vacancies with three vacancies, which supports the result that the vacancy clusters occlude vanadium tetrahedral ions at these compositions, as indicated by the negative values for $\alpha_{OT}^{MV_M}$ $(\frac{111}{444})$.

Table 9. *Possible stacking sequence of vanadium and oxygen vacancies in* VO_x $(x < 1)$

Z				Sequence
0	O	TC_1	$(TC_2 + TC_3 + TC_4)$	(1)
$\frac{1}{2}$	*M*	TA_1	$(TA_2 + TA_3 + TA_4)$	(2)
1	O	$(TB_2 + TB_3 + TB_4)$	TB_1	(3)
$1\frac{1}{2}$	*M*	$(TC_2 + TC_3 + TC_4)$	TC_1	(4)
2	O	TA_1	$(TA_2 + TA_3 + TA_4)$	(5)
$2\frac{1}{2}$	*M*	TB_1	$(TB_2 + TB_3 + TB_4)$	(6)
3	O	$(TC_2 + TC_3 + TC_4)$	TC_1	(7)
$3\frac{1}{2}$	*M*	$(TA_2 + TA_3 + TA_4)$	TA_1	(8)
4	O	TB_1	$(TB_2 + TB_3 + TB_4)$	(9)
$4\frac{1}{2}$	*M*	TC_1	$(TC_2 + TC_3 + TB_4)$	(10)
5	O	$(TA_2 + TA_3 + TA_4)$	TA_1	(11)
$5\frac{1}{2}$	*M*	$(TB_2 + TB_3 + TA_4)$	TB_1	(12)
6	O	TC_1	$(TC_2 + TC_3 + TC_4)$	(1)

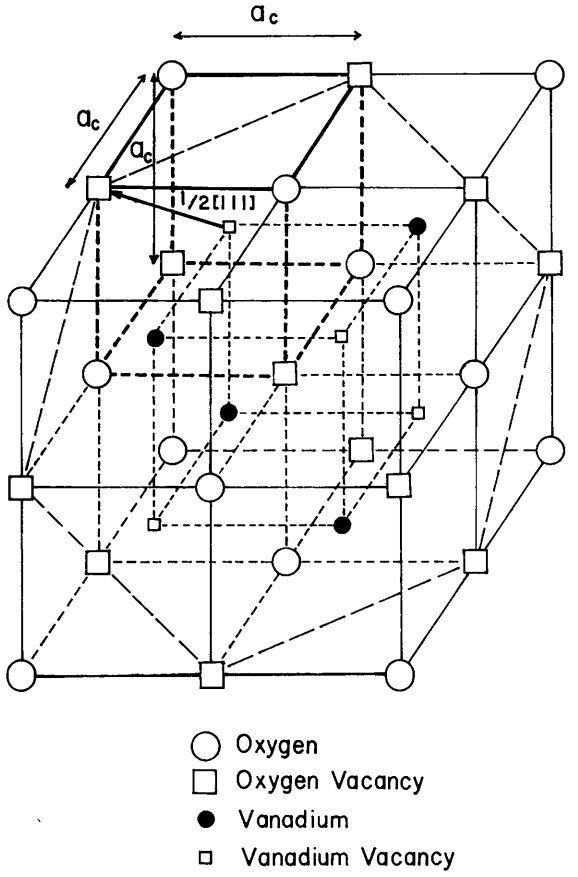

Fig. 12. A model of vacancy arrangements for VO_x for $x < 1$. The oxygen and vanadium vacancies are correlated in this model. Only the sites labeled (1) in Figs. 10 and 11 are shown, as the other sites are occupied by 'average' species (cation and cation vacancy or anion and anion vacancy).

Watanabe, Castles, Jostsons & Malin (1967) suggested that the ordered phase observed for $TiO_{0.9}$–$TiO_{1.1}$ below 1263 K has a structure in which half of the titanium and half of the oxygen ions are missing alternately on every third (110) plane, Fig. 13. This basic aspect of the ordering has been confirmed by Terauchi, Cohen & Reed (1978) and Terauchi & Cohen (1979) also showed that this tendency is present in the disordered phase. As shown in Fig. 13 for this phase, the near-neighbor vector between an oxygen vacancy (e.g. *A* in Fig. 13*b*) and a titanium vacancy (*B* or *C* in Fig. 13*a*) is $a_c/2$ [111], which coincides with the model for VO_x (see Fig. 12). Also, compare the square denoted by *OBDC* in Fig. 13(*a*) with Fig. 12 or Fig. 10(*a*). Some portions of the defect structure of VO_x for $x < 1$ are clearly similar to that in TiO_x.

For $x > 1$, the local order in VO_x is less extensive and there are indications that interstitials are associated with vacancies, as in Fe_xO (Koch & Cohen, 1969). It is interesting to note that for $x < 1$ VO_x is a semimetal like TiO_x, whereas for $x > 1$ it is a semiconductor like Fe_xO (Banus & Reed, 1970). The long-range electronic interactions that control the conductivity obviously have a strong effect on the local atomic arrangements.

Finally, we note that Ariya & Golomolzina (1962) suggest that VO contains regions like V_2O_3, based on infrared spectra. A comparison of Fig. 11(*d*), the V_2O_3 structure, with the domain model for VO_x, Fig. 11(*a*)–(*c*), does not indicate any such similarity.

Ionic displacements

From Fig. 5(*a*) it is clear that:

(*a*) $\bar{\gamma}_{lmn}$ varies with *lmn* as does α_{lmn};

(*b*) $\bar{\delta}^x_{100}$ is large;

(*c*) $\bar{\varepsilon}^{xy}_{lmn}$ for $lmn = \frac{1}{2}\langle 110\rangle$ (a first-neighbor vector) is large and negative.

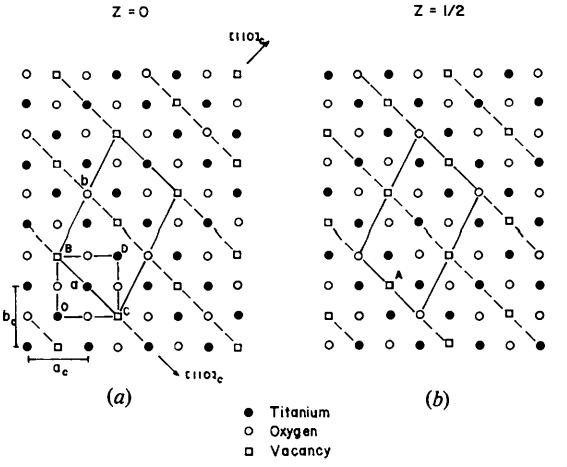

Fig. 13. Model of ordered TiO; (*a*) shows the $Z = 0$ plane and (*b*) shows the $Z = \frac{1}{2}$ plane. Solid lines represent the unit cell and dotted lines the planes containing vacancies.

Now:

(*a*) a positive $\bar{\gamma}^x_{lmn}$ means that the average distance between *lmn* neighbors is extended in the *x* direction, whereas a negative $\bar{\gamma}^x_{lmn}$ implies a contraction of the average inter-ion distance;

(*b*) a positive $\bar{\delta}^x_{lmn}$ implies that the ions connected by *lmn* are displaced in the same *x* direction, whereas a negative $\bar{\delta}^x_{lmn}$ corresponds to the case of displacements in the reverse direction;

(*c*) $\bar{\varepsilon}^{xy}_{lmn}$ has an analogous meaning to $\bar{\delta}^x_{lmn}$, but involves *x* and *y* components; $\bar{\delta}^x_{lmn}$ and $\bar{\varepsilon}^{xy}_{lmn}$ are related to thermal diffuse scattering (TDS) and Huang scattering.

Also, from Table 4*A* and *B*, $\bar{\gamma}^x_{lmn}$, $\bar{\delta}^x_{lmn}$ and $\bar{\varepsilon}^{xy}_{lmn}$ for type 1 vectors are combinations of displacements within the sublattices (*F*), (*O*) and (*T*). Although only coefficients for $VO_{1.17}$ have been presented, the experimental results (*a*)–(*c*) are the same for both $VO_{0.89}$ and $VO_{1.17}$ despite the interstitial concentration in $VO_{1.17}$. This indicates that there is little contribution of the displacements on the tetrahedral sublattice to the measured $\bar{\gamma}^x_{lmn}$, $\bar{\delta}^x_{lmn}$ and $\bar{\varepsilon}^{xy}_{lmn}$.

With this understanding, more information can be obtained from the measured coefficients, $\bar{\gamma}^x_{lmn}$, $\bar{\delta}^x_{lmn}$ and $\bar{\varepsilon}^{xy}_{lmn}$.

(*a*) When $\bar{\alpha}_{lmn}$ is negative, $\bar{\gamma}$ is negative (*e.g.* *lmn* = $\frac{1}{2}\langle 200\rangle$), indicating that as the number of vacancy–ion pairs increases, the average ionic distance decreases.

(*b*) $\bar{\delta}^x_{100}$ is large, compared with other $\bar{\delta}^x_{lmn}$. Komatsu & Teramoto (1966) report that there is strong thermal diffuse scattering at the 100 reciprocal-lattice position for NaCl-type crystals. This term is therefore undoubtedly related to thermal vibrations. It is interesting that the short-range order parameter $\bar{\alpha}_{100}$ has a large negative value for this vector. The preferential pairing of ions and vacancies between second-neighbor sites (see Fig. 10*a*) may be related to the lattice dynamics of the structure.

(*c*) The large negative value of $\bar{\varepsilon}^{xy}_{\frac{1}{2}\frac{1}{2}0}$ may be related to the preferential arrangements of vacancies along $\langle 110\rangle$ directions. As shown in Fig. 14, this coefficient can be due either to longitudinal or transverse displacements. The measured negative value for $\bar{\varepsilon}^{xy}_{\frac{1}{2}\frac{1}{2}0}$ means that case (*a*) and/or (*c*) occurs in disordered VO_x.

Simple considerations of the effective charge (or potential) at the vacant sites (*e.g.* see Swalin, 1961) allows speculation on these displacements. Cation vacancies and anion vacancies are likely to have effective negative and positive charges, respectively.

Either a vacancy–ion–vacancy sequence or a vacancy–vacancy–vacancy sequence might be expected from the domain model (Fig. 10*a*). As shown in Fig. 15, the ions are likely to be displaced due to their charges in the directions indicated by arrows. In Fig. 15(*b*), transverse displacements like those in Fig. 14(*c*) are present.

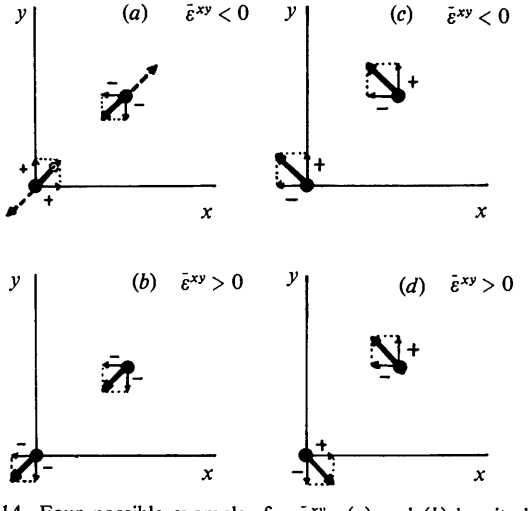

Fig. 14. Four possible examples for $\bar{\varepsilon}^{xy}_{\frac{1}{2}\frac{1}{2}0}$; (*a*) and (*b*) longitudinal components, (*c*) and (*d*) transverse components. When $\bar{\varepsilon}^{xy}_{\frac{1}{2}\frac{1}{2}0} < 0$, either case (*a*) or case (*c*) is possible.

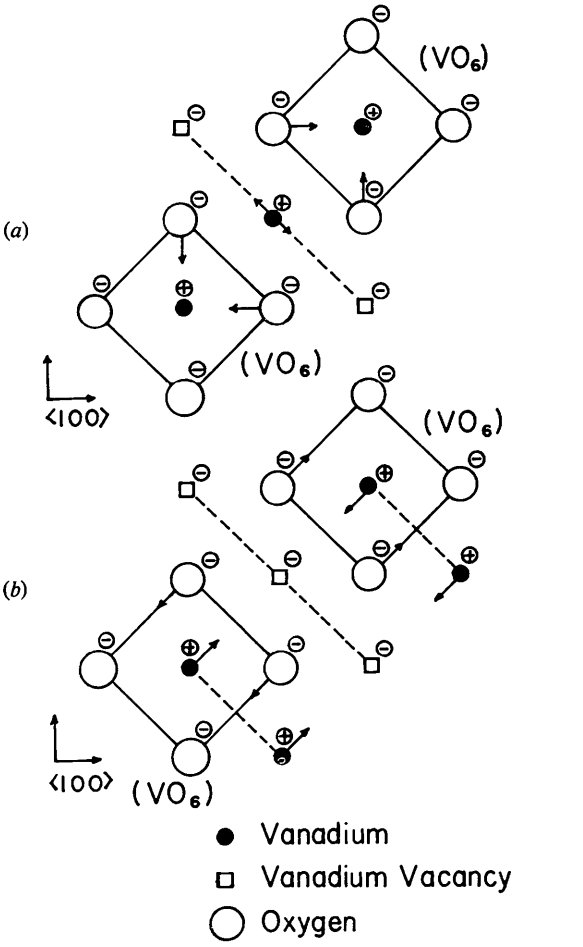

Fig. 15. The displacements of vanadium and oxygen ions due to a vacancy.

In the ordered phase (Part I), longitudinal displacements as in Fig. 14(*a*) were observed, but there are also transverse displacements as in Fig. 14(*d*), which are apparently not important in the disordered phase.

All the values of γ, δ, ε can be found in Morinaga (1978). The other parameters were small for all compositions. Only those listed in Fig. 5 were found to be important.

Physical properties

Goodenough (1972) has suggested that the large concentration of vacancies in this oxide permits a small lattice parameter and that this broadens the t_{2g} band, stabilizing occupied states. The increase in Madelung energy arising from the attendant charge distribution is apparently reduced in this system because the ions have nearly neutral charges (Morinaga & Cohen, 1976) and because of the wave-like arrangement of defects reported in this paper. As the first-neighbor short-range order parameter $\bar{\alpha}_{\frac{1}{2}\frac{1}{2}0} \simeq 0$ for VO_x (see Fig. 5), a vanadium ion is surrounded by the average concentration of vacancies. The bonding direction of t_{2g} orbitals is toward first-neighbor sites (Wollan, 1960), so that the bond distance between cations could be reduced by vacancies, while maintaining cubic symmetry. In agreement with this interpretation, it is known that VO_x has an unusually low lattice parameter compared to other transition-metal monoxides, and that high-pressure annealing, which reduces the vacancy content, increases the lattice parameter (Banus & Reed, 1970). However, the increase in strain energy due to the vacancies is also important. The association of the interstitial cations with vacancies reported here and in Part I minimizes this distortion. The V–O interatomic distances in V–O phases are summarized in Fig. 16 and it is clear that it is largest near the ordered phase $VO_{1.30}$, so that the driving force for ordering is probably largely to reduce strain energy, by ordering the displacements, perhaps due to vacancy–strain coupling as in TiO_x (Terauchi, Cohen & Reed, 1978).

Antiferromagnetism was detected in VO_x for $x > 1$ by Kawano, Kosuge & Kachi (1966) at 4–7 K, but this was refuted by Banus, Reed & Strauss (1972). For VO_x with a half-full and split t_{2g} band, antiferromagnetism might be expected for $x > 1$, because the transfer energy decreases with x (Goodenough, 1972). The possibility of electron tunneling between states localized at defects could eliminate the necessity of spin coupling between nearest neighbors (Anderson, 1958; Goodenough, 1972, 1973). But there is an additional reason that this might not occur. If, in Fig. 10(*b*), opposite spins are associated with a V ion and a vacancy (an electron trapping site), the spin arrangement is remarkably similar to that in other transition-metal monoxides. Although it is unknown what type of antiferromagnetism could occur in VO_x, the 180° cation–anion–cation superexchange interaction, which is so important in determining the magnetic behaviour in other transition-metal oxides, is undoubtedly weakened in VO_x by the large concentration of vacant cation sites.

This research was sponsored by the US Army Research Office (Grant No. DAAG-29-78-G-0156). The measurements were made in the long-term X-ray facility of Northwestern University's Materials Research Center, supported in part under the NSF-MRL program (Grant DMR-76-80847). This study constituted a portion of the PhD thesis submitted (by MM) in partial fulfilment of the requirements for the PhD degree at Northwestern University in March, 1978.

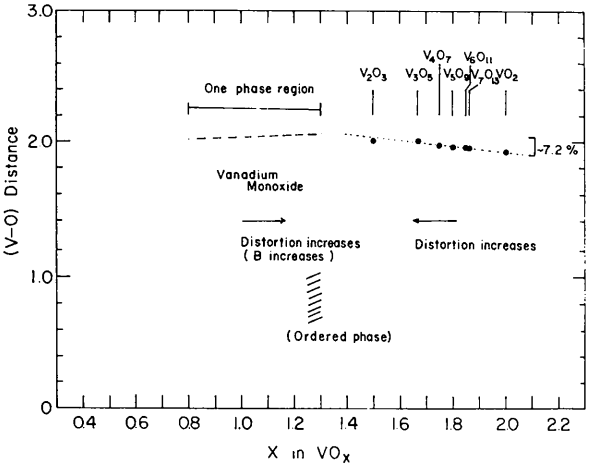

Fig. 16. Mean distance (V–O) in various vanadium oxide systems. Data on V_nO_{2n-1} were taken from Horiuchi, Morimoto & Tokonami (1976).

Note added in proof: simultaneously with this reseach, Andersson, Gjönnes & Forouh (1978) have speculated on the local defect arrays in disordered VO_x from considerations of the various ordered phases in the V–O system and of the symmetry of the diffuse electron scattering. They suggest a variation in the local defect arrangement with composition similar to that obtained from the quantitative studies reported here.

References

ANDERSON, P. W. (1958). *Phys. Rev.* **109**, 1492–1505.

ANDERSSON, B., GJÖNNES, J. & FOROUH, A. R. (1978). *J. Less Common Met.* **61**, 273–291.

ANDERSSON, B., GJÖNNES, J. & TAFTÖ, J. (1974). *Acta Cryst.* A**30**, 216–224.

ANDERSSON, B. & TAFTÖ, J. (1970). *Proc. Fifth European Congress on Electron Microscopy*, pp. 670–671.

ANDERSSON, G. (1954). *Acta Chem. Scand.* **8**, 1599–1606.

ARIYA, S. M. & GOLOMOLZINA, M. V. (1962). *Fiz. Tverd. Tela (Leningrad)*, **4**, 2921–2924.
BANUS, M. D. & REED, T. B. (1970). *The Chemistry of Extended Defects in Non-Metallic Solids*, edited by L. EYRING & M. O'KEEFE, pp. 488–522. Amsterdam: North-Holland.
BANUS, M. D., REED, T. B. & STRAUSS, A. J. (1972). *Phys. Rev. B*, **5**, 2775–2784.
BATTERMAN, B. W., CHIPMAN, D. R. & DEMARCO, J. J. (1961). *Phys. Rev.* **122**, 68–74.
BORIE, B. & SPARKS, C. J. (1971). *Acta Cryst.* A**27**, 198–201.
CROMER, D. T. (1969). *J. Chem. Phys.* **50**, 4857–4859.
DOYLE, P. A. & TURNER, P. S. (1968). *Acta Cryst.* A**24**, 390–397.
GEHLEN, P. C. & COHEN, J. B. (1965). *Phys. Rev. A*, **139**, 844–855.
GOODENOUGH, J. B. (1972). *Phys. Rev. B*, **5**, 2764–2774.
GOODENOUGH, J. B. (1973). *Defects and Transport in Oxides*, edited by M. S. SELTZER & R. I. JAFFEE, pp. 55–82. New York: Plenum.
GRAGG, J. E. JR (1970). PhD Thesis, Northwestern Univ., Evanston, Illinois 60201.
GRAGG, J. E. JR & COHEN, J. B. (1971). *Acta Metall.* **19**, 507–519.
HAYAKAWA, M. & COHEN, J. B. (1975). *Acta Cryst.* A**31**, 635–645.
HAYAKAWA, M., MORINAGA, M. & COHEN, J. B. (1973). *Defects and Transport in Oxides*, edited by M. S. SELTZER & R. I. JAFFEE, pp. 177–199. New York: Plenum.
HÖIER, R. & ANDERSSON, B. (1974). *Acta Cryst.* A**30**, 93–95.
HORIUCHI, H., MORIMOTO, N. & TOKONAMI, M. (1976). *J. Solid State Chem.* **17**, 407–424.
HUANG, K. (1947). *Proc. R. Soc. London Ser. A*, **190**, 102–116.
IIDA, S. (1955). *Progress of Magnetism*, edited by S. CHIKAZUMI, pp. 292–301 (in Japanese). Tokyo: Agne.
International Tables for X-ray Crystallography (1962). Vol. III. Birmingham: Kynoch Press.
KAWANO, S., KOSUGE, K. & KACHI, S. (1966). *J. Phys. Soc. Jpn*, **21**, 2744–2745.
KOCH, F. & COHEN, J. B. (1969). *Acta Cryst.* B**25**, 275–287.
KOMATSU, K. & TERAMOTO, K. (1966). *J. Phys. Soc. Jpn*, **21**, 1152–1159.
MORINAGA, M. (1978). PhD Thesis, Northwestern Univ., Evanston, Illinois 60201.
MORINAGA, M. & COHEN, J. B. (1976). *Acta Cryst.* A**32**, 387–395.
MORINAGA, M. & COHEN, J. B. (1979). *Acta Cryst.* A**35**, 745–756.
SCHÖNBERG, N. (1954). *Acta Chem. Scand.* **8**, 221–225.
SCHWARTZ, L. H. & COHEN, J. B. (1977). *Diffraction from Materials*. New York: Academic Press.
SCHWARTZ, L. H., MORRISON, L. A. & COHEN, J. B. (1963). *Adv. X-ray Anal.* **7**, 281–301.
STENSTRÖM, G. & WESTMAN, S. (1968). *Acta Chem. Scand.* **22**, 1712–1714.
SWALIN, R. A. (1961). *Thermodynamics in Solids*. New York: Wiley-Interscience.
TERAUCHI, H. & COHEN, J. B. (1979). *Acta Cryst.* A**35**, 646–652.
TERAUCHI, H., COHEN, J. B. & REED, T. B. (1978). *Acta Cryst.* A**34**, 556–561.
WATANABE, D., ANDERSSON, B., GJÖNNES, J. & TERASAKI, O. (1974). *Acta Cryst.* A**30**, 772–776.
WATANABE. D., CASTLES, J. R., JOSTSONS, A. & MALIN, A. S. (1967). *Acta Cryst.* A**23**, 307–313.
WESTMAN, S. & NORDMARK, C. (1960). *Acta Chem. Scand.* **14**, 465–470.
WILLIAMS, R. O. (1972). Report ORNL-4828. Oak Ridge National Laboratory, Tennessee.
WOLFF, P. M. DE (1956). *Acta Cryst.* **9**, 682–683.
WOLLAN, E. O. (1960). *Phys. Rev.* **117**, 387–401.

Acta Cryst. (1979). A**35**, 989–991

The Interpretation of Neutron Powder Diffraction Measurements on α-AgI

BY M. J. COOPER AND M. SAKATA*

*Materials Physics Division, AERE Harwell, Didcot OX*11 0*RA, England*

(*Received* 17 *January* 1979; *accepted* 22 *May* 1979)

Abstract

Recent neutron powder diffraction measurements on α-AgI by Wright & Fender [*J. Phys. C* (1977), **10**, 2261–2267] have been reanalysed using conventional least-squares analysis of the integrated Bragg intensities and have been shown to be consistent with other recent neutron diffraction measurements and with recent extended X-ray absorption fine structure (EXAFS) measurements. It is concluded that, although the distribution of silver ions within the unit cell can be modelled by locating isotropically vibrating ions in a number of crystallographic sites with partial occupancy, the most appropriate model is one in which the silver ions are located entirely in a single site but

* On leave from Nagoya University, Nagoya, Japan.

0567-7394/79/060989-03$01.00